Improvement of temperature homogeneity of a silicon wafer heated in a rapid thermal system (RTP: Rapid Thermal Process) by a filtering window

Pierre-Olivier Logerais [a, *], Olivier Riou [a], Fabien Delaleux [a], Jean-Félix Durastanti [a], Anne Bouteville [b]

[a] Centre d'Études et de Recherche en Thermique Environnement et Systèmes (CERTES), Université Paris-Est, IUT de Sénart, rue Georges Charpak, 77567 Lieusaint, France
[b] Laboratoire Arts et Métiers ParisTech d'Angers (LAMPA), 2, boulevard du Ronceray 49035 Angers Cedex 01, France

HIGHLIGHTS

- Heat transfer in a rapid thermal system (RTP: Rapid Thermal Process).
- Modelling with Monte Carlo method of the radiative heat transfer.
- Explanation of the silicon wafer temperature distribution.
- Temperature uniformity acquired by a filter on the underside of the quartz window.

Keywords:
RTP
Wafer temperature uniformity
Quartz window
Numerical simulation
Radiative properties
Filter

ABSTRACT

Rapid thermal processes are used in various key stages in the microelectronics industry. In this study, the heat transfer in a rapid thermal system is modelled with the finite volume method. The influence of the radiative properties of the quartz window on the thermal profile of the silicon wafer is first investigated. The obtained temperatures are interpreted by analyzing the radiative properties according to wavelength and temperature. The wafer temperature profile for a non-optimized heating in steady-state is explained by a four-phase scheme where the radiative heat fluxes are depicted. From this scheme, a filter on the underside of the quartz window is envisaged to achieve temperature uniformity for the wafer. Two configurations are tested, one where the filter covers the entire lower surface of the quartz window and another where it is placed in a ring close to the reactor wall to confine the infrared radiations with wavelengths beyond 2.6 μm in order to raise the temperature at the edge of the wafer. Simulations demonstrate that the latter modification enables a more significant improvement of the wafer temperature homogeneity with less than 1% dispersion. The implementation of the filtering window is also discussed.

1. Introduction

Rapid thermal processes (RTP) have been widely used in the manufacturing of microelectronic components. They are performed in different key stages such as annealing (ion implantation, dopant activation), oxidation or silicidation [1–3]. In the 1980s, the use of conventional furnaces started becoming a hindrance to the miniaturization of components due to their excessive inertia. Hence rapid thermal processes for which heating is provided by tungsten halogen infrared lamps and where the reactor wall is reflective and maintained at low temperature emerged to ensure precise heat treatments in the range of seconds or minutes [4,5]. The stringent requirement of less than 1 °C variation across the wafer (silicon substrate) enables to guarantee quality and long-term stability of the devices [6]. Many efforts have been attempted for the last 25 years to reach this requirement (Table 1) [7–14], but the

Abbreviations: CFD, computational fluid dynamics; DARTS, direct approach using ray tracing simulation; DTM, discrete transfer method; RTA, rapid thermal annealing; RTCVD, rapid thermal chemical vapour deposition; RTO, rapid thermal oxidation; RTP, rapid thermal process; SISO, single input single output; TCO, transparent conducting oxide.

* Corresponding author.
E-mail address: pierre-olivier.logerais@u-pec.fr (P.-O. Logerais).

Table 1
Evolution of the wafer temperature uniformity obtained in laboratory.

Process	Wafer		Temperature		Reference and date
	Diameter	Thickness	Set point	Deviation	
RTA	150 mm	675 μm	1100 °C	±2.8 °C	Keenan et al., 1991
RTP with control system	100 mm	525 μm	400–900 °C	±5 °C	Schaper et al., 1991
RTA	200 mm	725 μm	1000 °C	±2.4 °C	Gluck et al.
with lamp power correction				±1.2 °C	1999
RTA	300 mm	775 μm	1000 °C	±10.4 °C	
substrate rotation				±5.0 °C	
lamp power correction				±1.3 °C	
RTP with control:	200 mm	725 μm	600 °C	±0.358 °C	Huang et al.
multivariable 3×3			700 °C	±0.535 °C	2000
			800 °C	±0.751 °C	
			900 °C	±1.004 °C	
			1000 °C	±1.287 °C	
RTO	100 mm	525 μm	950–1010 °C	±10 K	Biro et al., 2002
Optimal design of RTP equipment	300 mm	775 μm	898	±4.4 °C	Kim 2002
RTP predictive model control	200 mm	725 μm	700 °C	±2 °C	Dassau et al., 2006
Spike annealing with control:	150 mm	675 μm	1000 °C		Jeng et al., 2013
SISO				±29 °C	
multivariable 2×2				±10 °C	
multivariable 3×3				±2.5 °C	

achievement of a uniform temperature at the surface of wafer still remains a challenge. The task becomes more and more difficult with the very tight thermal budgets of short processes like spike annealing and the increase of wafer diameters to fulfil the growing market demands [15].

Uniform temperature at the wafer surface is hard to obtain due to harsh power tuning of halogen infrared lamps, to the presence of edge effects for the wafer and to thermal gradients generated by the cold reactor wall [16,17]. Other effects are the convection in the reactor and not sufficiently high reflectivity of the reactor wall. An important constraint is the elevation of the temperature of the quartz window which acts on the distribution of the wafer temperature [18,19]. Moreover, contamination, aging, stability and placement of the wafer can also have an impact on the wafer temperature uniformity.

Various solutions have been deeply studied to obtain uniform wafer temperature as listed in Table 1, but they don't enable to achieve perfect temperature homogeneity and they usually remain very stringent [20]. Heating by several groups of lamps controlled separately allows getting uniform temperature at the surface of the wafer [9,10,21,22]. However, the mastering of the piloting requires a very thorough preliminary optimization and aging of the lamps is accelerated for the ones supplied with higher power. Rotating the wafer allows to homogenize the temperature circularly but the temperature difference between the centre and the edge of the wafer stays unchanged [9,23,24]. Using a susceptor enables to get a better temperature homogeneity [25], nevertheless the addition of a susceptor has the drawback of reducing the rapidity of the heating because thermal inertia becomes more important. The use of a guard ring placed around the silicon substrate permits to reduce edge effects [26]. It has several inconveniences like difficult handling of the wafers during loading, augmentation of the reactor size and deposition on the ring which enhance the risk of contamination of the wafers. A diminution of the wafer temperature differences is also obtained by increasing the reflectivity of the wall of the reactor to direct the radiations towards the wafer edge [6,27].

Numerical modelling has proved to be a precious aid to identify, depict and quantify the heat and mass transfers in processes. It permits to diminish the number of experimental trials and to investigate on the sensitivity of parameters. Radiative heating of the silicon wafer has been numerically modelled by different methods with the aim of better understanding and uniforming the wafer temperature in RTP systems. Solutions of the energy balance equation for the wafer have been determined in numerous studies by calculating view factors between the lamp array divided in heating zones and wafer slices. The solutions are either used to optimize the design of the reactor chamber [28–30] or to predict the lamp power to supply in order to control the transient evolution of the wafer temperature [12,13,31]. To simulate the solution of the radiative heat transfer from the tungsten filament halogen lamps to the silicon wafer, ray tracing methods have been implemented. A direct approach model using the three-dimensional ray-tracing simulation (DARTS) was developed by Habuka et al. [32]. The paths of the infrared rays emitted from the lamps are traced following reflections at the surface of the specular reflectors until they reach the silicon wafer. The absorbed ray intensities calculated for the silicon wafer have been related to measured temperatures of the silicon wafer with the Stefan–Boltzmann law and heat losses caused by the reflective wall have been quantified. Discrete transfer methods (DTM) which consist in discretizing the solid angle into ray directions allow to take into account spectral, specular or diffuse properties of surfaces to display a solution to the radiation transport equation [33,34]. Ray tracing with Monte Carlo statistical method enables to take into consideration most of the radiation phenomena by describing the radiative heat exchange by means of a matrix whose coefficients depend on the disposition of one surface to the other and on the spectral and temperature radiative properties, namely the emission and the reflection ones (partially or totally specular or diffuse). The main advantages regarding other approaches is the faithful restitution of diffuse character of surfaces and also the following of elevated number of representative rays [35–37]. The radiative heat transfer resolution must be coupled with the conductive and convective heat transfer solving. The finite volume method is well suited for this coupling as it is robust to solve conservation relations. The partial differential equations are indeed integrated on each control volume and the integral of the divergence term is converted to a surface integral. Fluxes are then evaluated at the interfaces between adjacent finite volumes. As the flux entering a given volume is equal to the outward one, the conservation is excellently accounted for.

In the present study, the heating of the silicon wafer by tungsten filament halogen infrared lamps is investigated by utilizing a Computational Fluid Dynamics (CFD) approach. In a previous study, a rapid thermal equipment had been modelled and validated [38].

The first numerical simulations enabled to show that the presence of the quartz window and its low diffusivity largely conditions the shape of the temperature profile of the silicon wafer [19,39,40]. Hereafter, numerical simulations are carried out using the validated model to better understand the radiative heat exchanges between the heated wafer and the quartz window. For this purpose, the radiative properties of the wafer are modified and simulations of its heating are performed for each modification. The shape of the temperature distributions of the silicon wafer and the one of the quartz window are explained with an analysis of the radiative properties of participating surfaces. The analysis is extended to offer solutions to acquire wafer temperature uniformity. The effectiveness of the proposed solutions is discussed based on numerical simulations integrating the modifications. Lastly, the feasibility is shown with technical considerations from literature.

2. Modelling

2.1. Rapid thermal system

The modelled rapid thermal system is the one of an equipment type AS-150 marketed by the company AnnealSys (Montpellier, France). It enables to perform annealing, oxidation, diffusion, silicidation and nitridation [41]. The two-dimensional model with the computational domain is shown in Fig. 1. The furnace contains a bench of eighteen tungsten filament halogen infrared infrared lamps. The reactor is of cylindrical shape and its wall is kept cooled at 300 K by a water flow. A silicon wafer of 150 mm diameter (6 inches) and 500 μm thickness is placed in the reactor on three quartz pins. A quartz window seals the reactor and lets the infrared radiations from the tungsten halogen lamps around 1 μm wavelength pass through in order to heat the silicon wafer. A gas pumping system is used to maintain the gas in the reactor at reduced pressure. A panel permits to control the injection and the exhaust of gases. In our case, the silicon wafer is placed in a nitrogen atmosphere at a pressure of 300 Pa.

2.2. Equations

The conservation equations that govern heat and mass transfers are solved with the finite volume method [42]. The conservation equations are integrated over each control volume of the domain. The grid is regular as depicted in Fig. 1. The grid configuration includes a sufficient number of balanced square shape control volumes, which is well suited for the finite volume resolution. 94% of the 4598 control volumes are of square shape with a side of 2.5 mm to limit both the errors of discretization and the ones of rounding of the digital resolution. This size also enables to have acceptable computational times. Besides, the injection part and the wafer are slim and adapted control volumes permit to ensure precise velocity and temperature distributions.

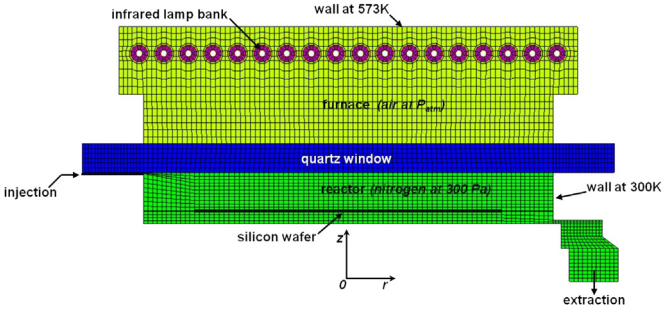

Fig. 1. Modelling of the rapid thermal equipment with the computational domain.

The mass conservation equation and the momentum conservation equation in the steady-state for cylindrical coordinates are respectively given by expressions (1) and (2):

$$\frac{1}{r}\frac{\partial}{\partial r}(r\rho v_r)+\frac{1}{r}\frac{\partial}{\partial \theta}(\rho v_\theta)+\frac{\partial}{\partial z}(\rho v_z)=0 \tag{1}$$

$$\begin{cases}\frac{1}{r}\frac{\partial}{\partial r}(r\tau_{11})+\frac{1}{r}\frac{\partial}{\partial \theta}(\tau_{12})+\frac{\partial}{\partial z}(\tau_{13})-\frac{1}{r}\tau_{22}=f_r\\ \frac{1}{r}\frac{\partial}{\partial r}(r\tau_{21})+\frac{1}{r}\frac{\partial}{\partial \theta}(\tau_{22})+\frac{\partial}{\partial z}(\tau_{23})+\frac{1}{r}\tau_{21}=f_\theta\\ \frac{1}{r}\frac{\partial}{\partial r}(r\tau_{31})+\frac{1}{r}\frac{\partial}{\partial \theta}(\tau_{32})+\frac{\partial}{\partial z}(\tau_{33})=f_z\end{cases} \tag{2}$$

The heat transfer is calculated by solving the energy conservation equation (3) in steady-state:

$$\begin{aligned}&\frac{1}{r}\frac{\partial}{\partial r}\left\{r\left[(\rho E+p)v_r-(\tau_{11}v_r+\tau_{21}v_\theta+\tau_{31}v_z)-k\frac{\partial T}{\partial r}\right]\right\}\\&+\frac{1}{r}\frac{\partial}{\partial \theta}\left[(\rho E+p)v_\theta-(\tau_{12}v_r+\tau_{22}v_\theta+\tau_{32}v_z)-\frac{k}{r}\frac{\partial T}{\partial \theta}\right]\\&+\frac{\partial}{\partial z}\left[(\rho E+p)v_z-(\tau_{13}v_r+\tau_{23}v_\theta+\tau_{33}v_z)-k\frac{\partial T}{\partial z}\right]\\&=f_rv_r+f_\theta v_\theta+f_zv_z+S_e\end{aligned} \tag{3}$$

in which E is the total specific energy defined by the following expression (4):

$$E=e+\frac{1}{2}v^2 \tag{4}$$

Radiative heat exchanges are simulated using the Monte Carlo method whose principle is to follow the fate of packets of photons emitted by the various internal surfaces [43]. The rays emitted by a surface are traced until they are absorbed by the same surface or another one. Surfaces are discretized in "patches". The radiative heat flux for a patch i is the result of incident radiation from all other patches j and from its own emission:

$$Q_i=q_iA_i=\sum_{j=1}^{N_S}(M_{ij}-\delta_{ij}\varepsilon_j)\sigma T_j^4A_j \tag{5}$$

The found solution is reported in the source term S_e of the energy transfer equation (3) in order to combine radiative, convective and conductive heat transfers to determine the temperature distribution on the overall domain.

A packet of photons emitted from a patch i is either reflected or transmitted by the different encountered bodies before being absorbed. Each of these events depends on the wavelength of the beam, its direction of propagation, the orientation of the surfaces and their temperatures. The radiative properties can be defined by knowing the complex refractive indices of the materials:

$$\tilde{n}_\lambda=n_\lambda-ik_\lambda \tag{6}$$

For many materials, the complex index of refraction depends on the temperature T and can be expressed in a polynomial form:

$$\begin{cases}n_\lambda=n_0+n_1\theta+n_2\theta^2+n_3\theta^3\\ k_\lambda=\left(k_1+k_2\theta+k_3\theta^2\right)\cdot\exp[k_0\theta]\end{cases} \tag{7}$$

where n_0, n_1, n_2, n_3, k_0, k_1, k_2 and k_3 are the coefficients of monomials and $\theta=(T-300)/1000$ is the reduced temperature.

Absorptivity, emissivity, reflectivity and transmissivity are calculated for the surfaces of semi-transparent parallel solids (silicon substrate, quartz window, quartz bulb of infrared lamps) and for opaque surfaces (reactor wall, tungsten filament, injection and exhaust of gases). In the case of semi-transparent solids, the absorption is assumed constant in the whole bulk. The spectral transmissivity τ_λ between two points x and y depends on the distance traversed through the material but not on the direction:

$$\tau_\lambda = e^{-4\pi k_\lambda |x-y|/\lambda} \tag{8}$$

The spectral reflectivity ρ_λ is calculated with the Fresnel formulae:

$$\rho_\lambda = \frac{1}{2}\left(\frac{\tan^2(\theta_1-\theta_2)}{\tan^2(\theta_1+\theta_2)} + \frac{\sin^2(\theta_1-\theta_2)}{\sin^2(\theta_1+\theta_2)}\right) \tag{9}$$

in which θ_1 is the incidence angle and θ_2 is the refraction angle. When a refracted incident ray passes from a dielectric medium having a refractive index n_λ to another one with refractive index n'_λ, both the angles are related by the Snell law:

$$n_\lambda \sin\theta_1 = n'_\lambda \sin\theta_2 \tag{10}$$

Knowing τ_λ and ρ_λ, the absorptivity α_λ is deduced:

$$\alpha_\lambda = 1 - \rho_\lambda - \tau_\lambda \tag{11}$$

The total hemispherical absorptivity $\alpha_{\theta,\lambda}$ is equal to the total hemispherical emissivity $\varepsilon_{\theta,\lambda}$ (Kirchhoff's law), so for a wavelength λ and for an angle θ at equilibrium:

$$\alpha_{\theta,\lambda} = \varepsilon_{\theta,\lambda} \tag{12}$$

In the case of opaque surfaces, especially metal surfaces, the reflectivity is deduced from the Fresnel relations:

$$\rho_{\lambda,\theta} = \frac{1}{2}\left(\frac{(n_\lambda\cos\theta-1)^2+(k_\lambda\cos\theta)^2}{(n_\lambda\cos\theta+1)^2+(k_\lambda\cos\theta)^2} + \frac{(n_\lambda-\cos\theta)^2+k_\lambda^2}{(n_\lambda+\cos\theta)^2+k_\lambda^2}\right) \tag{13}$$

Since the transmissivity $\tau_\lambda = 0$, the absorptivity and the total hemispherical emissivity are equal to:

$$\alpha_{\theta,\lambda} = \varepsilon_{\theta,\lambda} = 1 - \rho_{\lambda,\theta} \tag{14}$$

A beam contains billions of photons, therefore the calculations have to be restricted to a limited number of photons which have to be representative with perfectly randomized trajectories in the case of diffuse properties. Bundles of photons are then considered with attributed emission point, direction and wavelength. These characteristics are determined by using the spectral distribution of the emissive power. To determine for example the wavelength, the distribution of the emissive power is divided into N energy packets, each one of them defined for a wavelength domain between 0 and λ. The probability that a photon bundle has a wavelength between 0 and λ is given by the cumulative distribution function:

$$R_\lambda(\lambda) = \int_0^\lambda P(\lambda)\mathrm{d}\lambda = \frac{\int_0^\lambda E_\lambda \mathrm{d}\lambda}{\int_0^\infty E_\lambda \mathrm{d}\lambda} \tag{15}$$

The cumulative distribution function R_λ varies between 0 and 1. This way, randomly generating R_λ is possible and representative. By inverting equation (15), for a value $R_{\lambda 0}(\lambda,)$, a wavelength λ_0 is obtained. By performing random draws for numerous values of $R_\lambda(\lambda)$, drawn numbers between 0 and 1, a set of representative wavelengths is obtained by the inverse function R_λ^{-1}. The other characteristics of the photon bundle are generated by inverting the associated cumulative distribution function. First, the coordinates of the emission points are determined, then the wavelength and the emission direction. Thus, the random character of the diffuse emission or reflection can be modelled. Once a packet of photons reaches a point of a surface, it is either absorbed, reflected or transmitted. The ray tracing and the intersection points with a surface are determined using the scalar product of a normal vector to the surface with a vector having the direction of the photon [44].

2.3. Properties

The solving of equations (1)–(3) requires the volume properties (density, specific heat capacity and thermal conductivity) of the tungsten filament, the quartz of the lamp bulb and of the window, the air in the furnace and the nitrogen in the reactor. These properties with their temperature dependence are all defined in Ref. [38]. For the silicon wafer, the density is of 2329 kg m^{-3}. The specific heat capacity and the thermal conductivity of silicon are provided according to temperature in Fig. 2 [45,46]. The initial temperature of the system is of 300 K. The boundary conditions with the radiative properties of each surface to calculate relation (5) are indicated in Table 2.

3. Numerical simulations

Numerical simulations of the rapid thermal system are performed using CFD'Ace software [47,48]. The properties of each surface in Table 2 are listed in a "patch" file in which all the coefficients of the monomials of equation (7) are stored according to wavelength (one hundred values between 0.1 μm and 100 μm). One file is assigned to the solver for each boundary condition. The emission of 5 million rays is interesting to have a sufficient number of photons for each patch. There cannot be more patches than adjacent cells to a surface and a compromise must be found between the patch size and a sufficient number of traced rays reaching the patch in order to determine accurately the radiative fluxes. The number of patches has been optimized for the wafer surface (30 patches) to dispose of accurate temperature distributions.

Ray tracing is performed to simulate the radiative heat exchange given by equation (5). The balance of radiative fluxes is determined for all the control volumes until the global equilibrium of heat fluxes is reached, in other words, when the residue is reduced by four orders of magnitude of the initial value or more. It is necessary to restart a release of 5 million rays every 400 iterations to have enough traced rays in the numerical solving of conservation equations. Resolution takes 15 min (about 1200 iterations) for a simulation in the steady-state case performed with a calculating unit of 1 GB RAM which is adequate for ray tracing of the Monte Carlo method and integration of each conservation equation on each control volume. Concordance with experimental results and 3D model was shown in Ref. [38].

We deliberately consider the case where the lamp heating is not optimized in steady-state in order to dispose of the biggest spatial temperature variations for the wafer and therefore grasp the sensitivity of the modified parameter. The calculations are performed for different lamp heating powers (10–30%) in the steady-state. As the aim is to better understand the radiative heat exchange between the silicon substrate and the quartz window, numerical simulations are first carried out by changing the radiative property of the substrate. The four treated cases are shown in Table 3 which indicates the magnitudes of the emissivity, the absorptivity and the reflectivity.

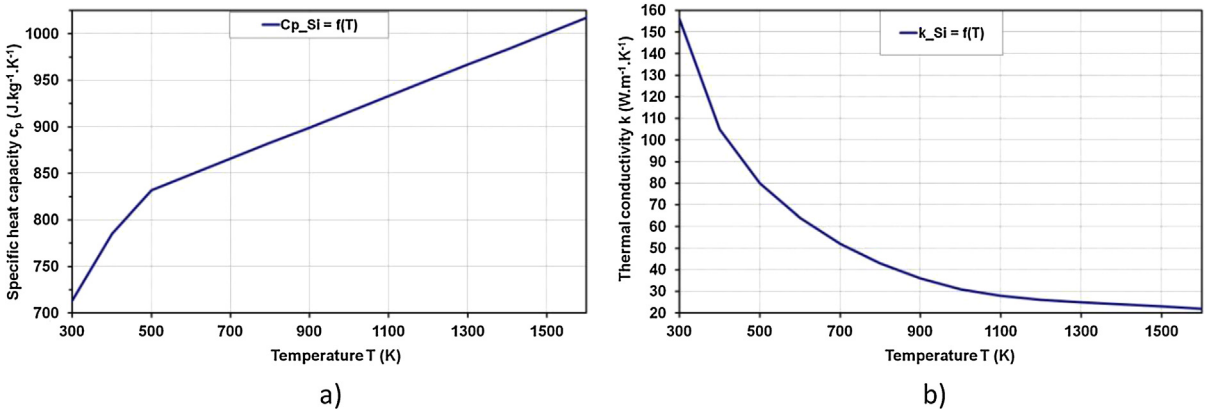

Fig. 2. Specific heat capacity and thermal conductivity of silicon wafer [45,46].

4. Temperature profiles

4.1. Analysis

The temperatures at the centre of the quartz window and at the centre of the substrate were taken according to the lamp heating power (Fig. 3). The substrate and the window are the hottest in the case where the substrate has the property of a blackbody. The temperatures of the substrate and of the quartz window depend on the absorptivity and on the emissivity of the substrate. The more they are important, the higher the temperatures get [17]. Thus, the quartz window is heated by the radiations emitted by the substrate. When the substrate has the property of a perfect reflector, its temperature is of about 520 K. As the substrate reflects on the entire spectral range, we were expecting to obtain a temperature close to 300 K. The substrate is indeed heated by convection because there is hot nitrogen in the reactor. The temperature of the quartz window is higher than in the case of silicon when the reflectivity of the substrate is of 100% for all the wavelengths. When considering the absence of substrate, the radiations reflected by the reactor wall towards the quartz window are absorbed by the latter which results in its temperature raise. Nevertheless, the increase in temperature is less important than in the case of a perfectly reflective substrate because the reactor wall absorbs one part of the radiations (absorptivity of 0.25).

Table 2
Boundary conditions.

Surface	Type	Radiative property	Temperature
Filament (lamp)	Wall	Tungsten	According to power
Bulb	Interface	Quartz	300 K < T < 1500 K
Window	Interface	Quartz	300K < T < 1500 K
Wafer	Interface	Silicon	300K < T < 1500 K
Furnace	Wall	Stainless steel	573 K
Reactor	Wall	Stainless steel	300 K
Injection	Inlet	Blackbody	300 K
Exhaust	Outlet	Blackbody	300 K

Table 3
Magnitude of radiative properties of the substrate.

Case	1	2	3	4
	Without wafer (reactor wall)	Silicon	Perfect reflector	Blackbody
Emissivity $\varepsilon_{\theta,\lambda}$ = absorptivity $\alpha_{\theta,\lambda}$	0.25	0.7	0	1
Reflectivity ρ_λ	0.75	0.3	1	0

4.2. Explanation

The radiative properties of surfaces according to wavelength are analyzed with more details to explain the effect of the substrate emissivity and reflectivity on the temperature of the quartz window, and the one of the reactor wall. Fig. 4 shows these properties at normal incidence [49], the values remaining almost similar for oblique incidences.

The case for which the substrate has the radiative properties of the blackbody and the one for which it has the ones of silicon are

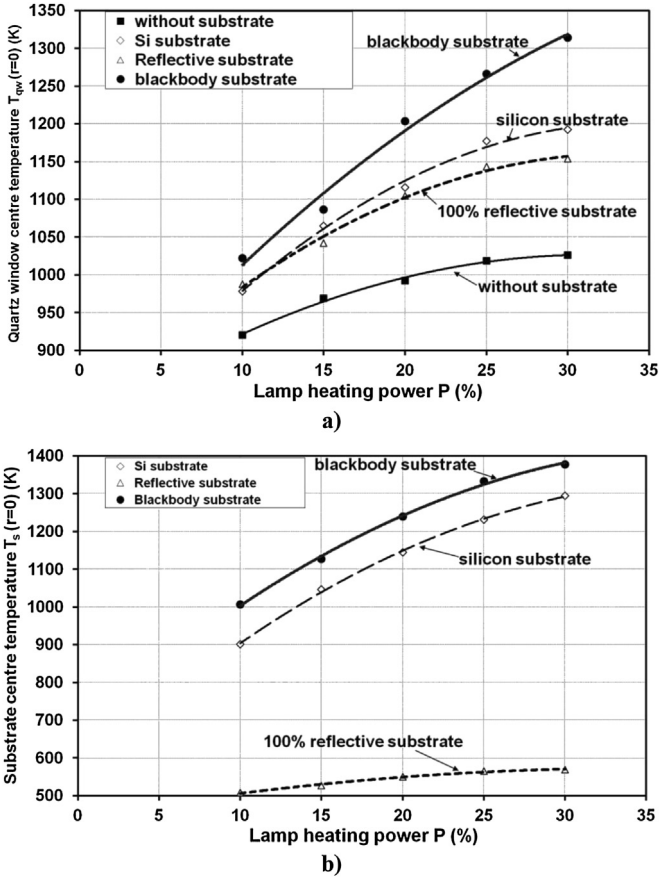

Fig. 3. Temperature at the centre of the quartz window (a) and at the centre of the substrate (b) according to the lamp heating power.

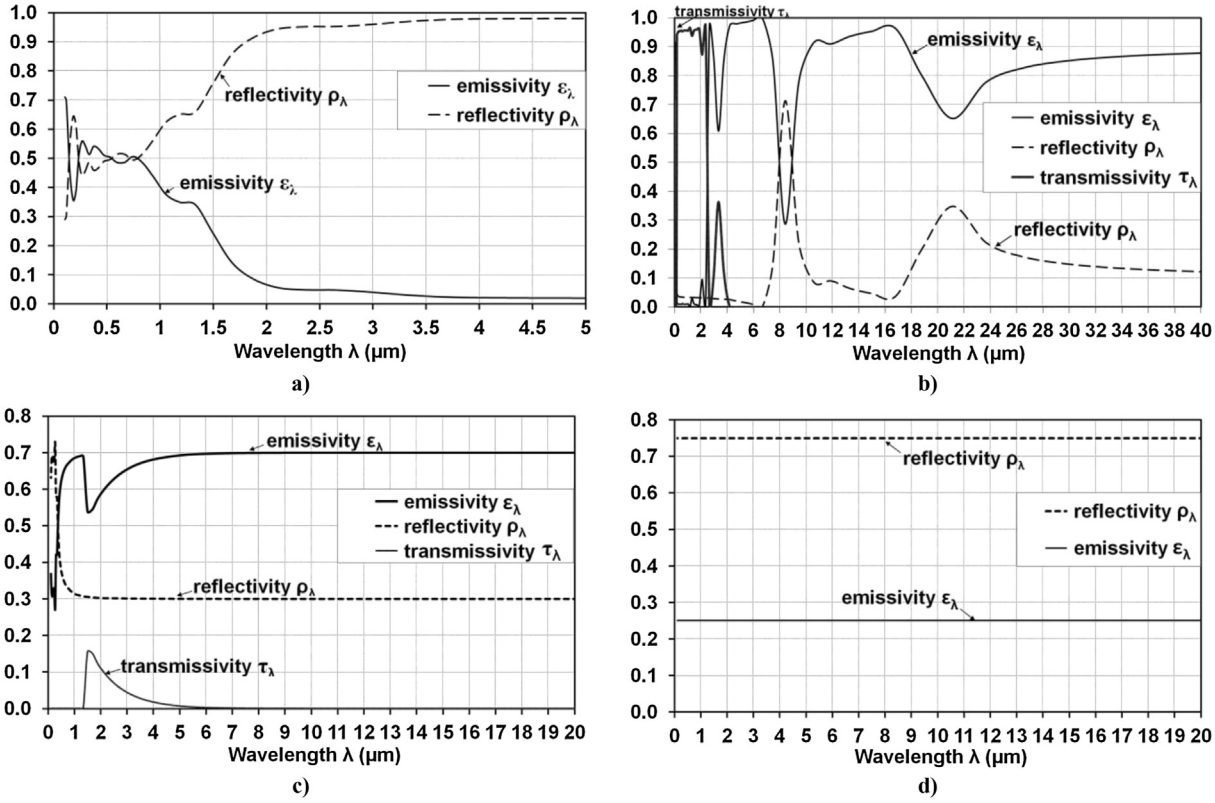

Fig. 4. Radiative properties of tungsten of halogen lamps (a), of quartz window (b), of silicon substrate at 1000 K (c) and of stainless steel of the wall (d).

first confronted. When the substrate has the property of a blackbody, it absorbs all the radiations emitted by the tungsten halogen lamps that it receives. Hence it becomes hotter than in the case of the silicon substrate for which the absorptivity is of 0.7. The hot blackbody substrate emits over the entire spectral range, emissivity of 1 against 0.7 for silicon. The quartz window absorbs strongly for wavelengths beyond 2.6 μm. It is therefore heated by the radiations emitted by the substrate with wavelengths beyond 2.6 μm. The temperature of the quartz window is higher in the case of the substrate having the characteristics of a blackbody because of its more important emission. The temperature of the quartz window depends on the emissivity of the substrate.

The case without substrate and the one where the substrate is perfectly reflective are compared hereafter. The quartz window absorbs with a small percentage, about 5%, the radiations centred at around 1 μm wavelength emitted by the tungsten halogen lamps. It absorbs in the same proportion the reflected radiations by the reactor wall. As the calculations were carried out for the steady-state case, for an infinite assumed time, the quartz window had sufficient time to absorb radiations to reach a high stabilized temperature. The temperature of the quartz window is higher when the substrate is perfectly reflective because the latter returns more radiations than in the case where there is no substrate. The reactor wall has a smaller reflectivity (0.75). The rest of the radiations are absorbed (absorptivity of 0.25), but the emitted flux is low because the temperature is of 300 K. The silicon substrate reflects 30% of the radiations it receives from the tungsten halogen lamps and the quartz window absorbs with a nether coefficient of 5% but for a sufficient time to elevate its temperature. Definitely, the radiations centred at around 1 μm wavelength provided by the tungsten halogen lamps which are reflected by the substrate heat the quartz window as well.

4.3. Heat transfer scheme

Using the previous conclusions, the shape of the temperature distribution for the silicon wafer and the quartz window in steady-state can be explained with a four-phase scheme (Fig. 5). The temperature profiles in the scheme are represented in a relative way:

$$\begin{cases} T_{s,\mathrm{rel}} = \dfrac{T_s(r) - T_{s,\mathrm{edge}}}{T_s(r=0) - T_{s,\mathrm{edge}}} \\ T_{qw,\mathrm{rel}} = \dfrac{T_{qw}(r) - T_{qw,\mathrm{edge}}}{T_s(r=0) - T_{qw,\mathrm{edge}}} \end{cases} \tag{16}$$

The r coordinate corresponds to the radial position at the surface of the wafer and at mid height of the quartz window. The reference $r = 0$ is taken at the centre of the wafer and at the one of the quartz window. The orientation is indicated in Fig. 1. The index "s" for substrate is preferred to "w" for wafer not to mix up with the notation "qw" of the quartz window.

- *Phase 1*

The tungsten halogen lamps emit a radiative heat flux centred at around 1 μm wavelength which is 95% transmitted through the quartz window.

- *Phase 2*

The radiative heat flux is 70% absorbed and 30% reflected by the silicon wafer. The latter emits on the whole infrared domain (emissivity of 0.7). The emitted flux is directed towards the quartz window and the wall of the reactor at 300 K. The net heat flux exchanged between the edge of the hot wafer and the wall

at 300 K is important. The wafer temperature is lower at its edge than at its centre because of the incident radiative heat flux distribution provided by the bank of lamps, the convective losses and the conductive heat flux from the centre to the edge of the wafer. Indeed, there are convection cells in the reactor where nitrogen gas flows due to temperature differences between the edge of the wafer, the hot quartz window, the cooled reactor wall, the injection and the exhaust [39]. As the wafer temperature is lower at its edge, the flux emitted by the wafer is greater at its centre. One part of the emitted radiations by the edge of the wafer is reflected or absorbed by the reactor wall and one part is reflected in direction of the underside of the quartz window namely, in the area close to the reactor wall.

- *Phase 3*

The quartz window absorbs 80% of the radiations emitted by the silicon wafer having wavelengths beyond 2.6 μm and reflects the rest. Since the received flux at the centre of the quartz window is more important than at its edge, the temperature window becomes even higher at its centre. The centre-to-edge temperature difference of the quartz window is enhanced by the conductive heat flux towards its outer edge.

- *Phase 4*

The radiations absorbed by the quartz window are re-emitted towards the wafer and the reactor wall (emissivity of 0.8). As the temperature of the quartz window is higher at its centre, the flux emitted by the quartz window towards the centre of the wafer is greater than the one at its edge. Thus, the temperature difference between the centre and the edge of the wafer is even further increased. The hot quartz window also emits towards the reactor wall. Some rays are hence reflected in direction of the wafer edge but the heat flux is not sufficient to balance the losses at the wafer edge.

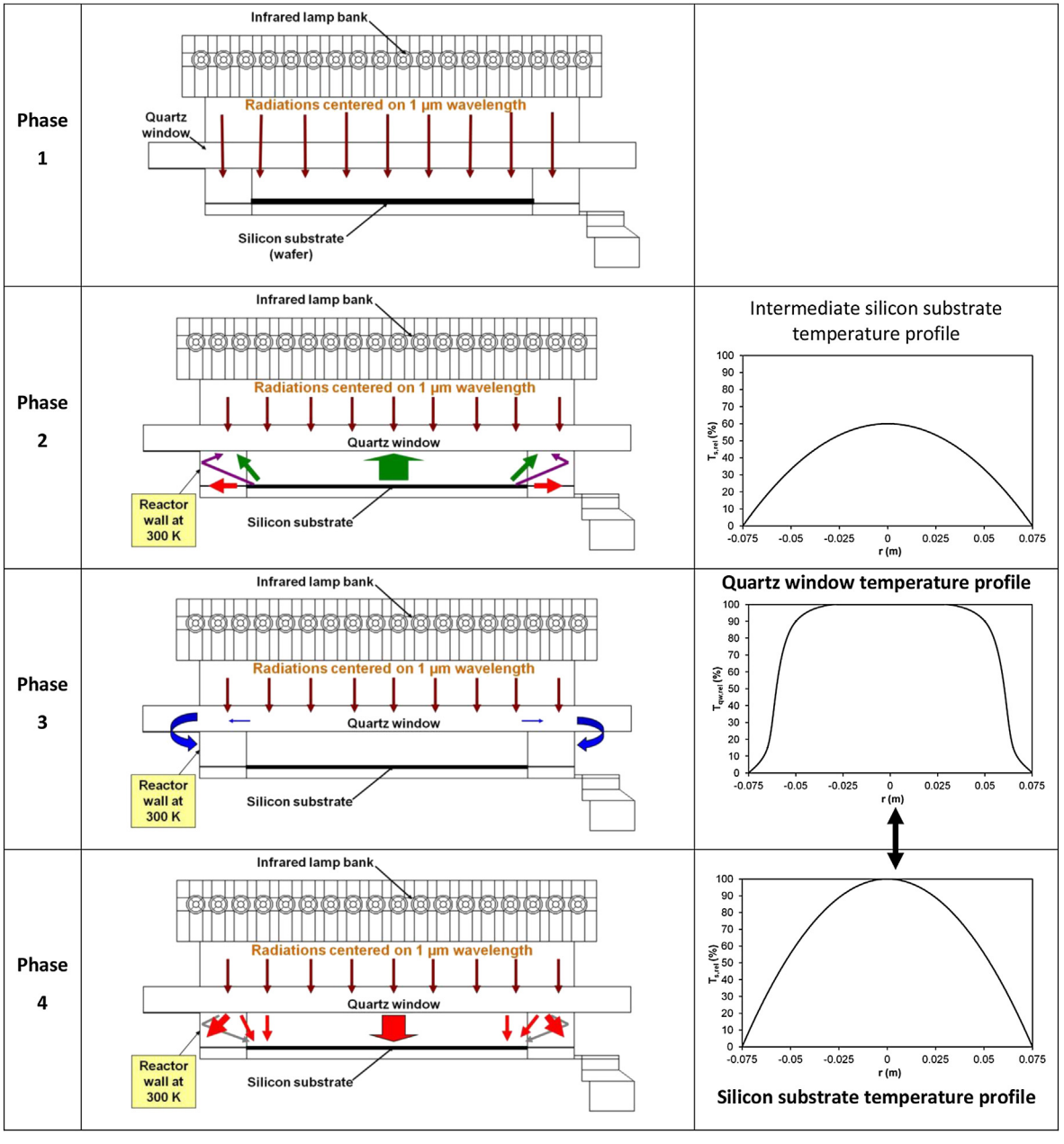

Fig. 5. Explanation of the shape of temperature profiles of the silicon substrate and of the quartz window in steady-state.

5. Solution schemes

To achieve a uniform surface temperature at the surface of the wafer, unbalanced heat fluxes have to be compensated. Reasoning on the heat transfer scheme, two propositions are formulated hereafter.

5.1. Scheme 1

To prevent overheating of the quartz window, it would be interesting to block the absorption on the underside of the quartz window for radiations with wavelengths beyond 2.6 μm emitted by the silicon wafer and to let radiations emitted by the tungsten halogen lamps centred at around 1 μm wavelength, be transmitted. A way must be found to reflect on the underside of the quartz window the radiations emitted by the silicon wafer with wavelengths beyond 2.6 μm (Fig. 6a). The temperature gradients of the quartz window would hence be reduced, which should give a more homogeneous wafer temperature.

5.2. Scheme 2

It has been shown in phase 2 that the area of the quartz window close to the reactor wall receives an important part of the radiations emitted by the edge of the wafer, either directly or by a reflection on the reactor wall. Radiations having wavelengths beyond 2.6 μm incident on the quartz window are absorbed by 80%. The quartz window emission is limited in this area because the temperature is relatively low due to both the proximity of the cooled reactor wall and the presence of a conductive flux towards the outer edge of the quartz window. It would then be interesting to reflect the radiations with wavelengths beyond 2.6 μm as in Scheme 1 but only in the region neighbouring the reactor wall and redirect the radiative heat flux towards the edge of the wafer to balance the losses (Fig. 6b). Two paths are possible for the reflected rays (Fig. 7):

- emission of the wafer, reflection at the surface of the window close to the reactor wall and reflection on the reactor wall and way back to the edge of the wafer (path 1)
- emission of the wafer, reflection on the reactor wall and reflection at the surface of the window close to the reactor wall and way back to the edge of the wafer (path 2).

A priori, the reflected flux arriving at the edge of the wafer should be sufficient to offset the losses. By reasoning on the magnitude of radiative heat fluxes (see diagrams of Fig. 8), both propositions seem worth exploiting. Radiations from the lamps with wavelengths below 2.6 μm are transmitted by the quartz window (95% of transmission) and are incident on the wafer.

For the first proposition (Fig. 8a), in the wavelength domain beyond 2.6 μm, the flux emitted and reflected by the wafer at its centre is in the same magnitude as the flux reflected at the centre of the window. In the same manner, the flux emitted and reflected by the wafer at its edge is in the same magnitude as the flux reflected in the part of the window closer to the reactor wall. However, the emitted and reflected flux by the wafer at the edge is inferior to the one at its centre. Hence, the flux reflected by the quartz window surface closer to the reactor wall is inferior to the one reflected by

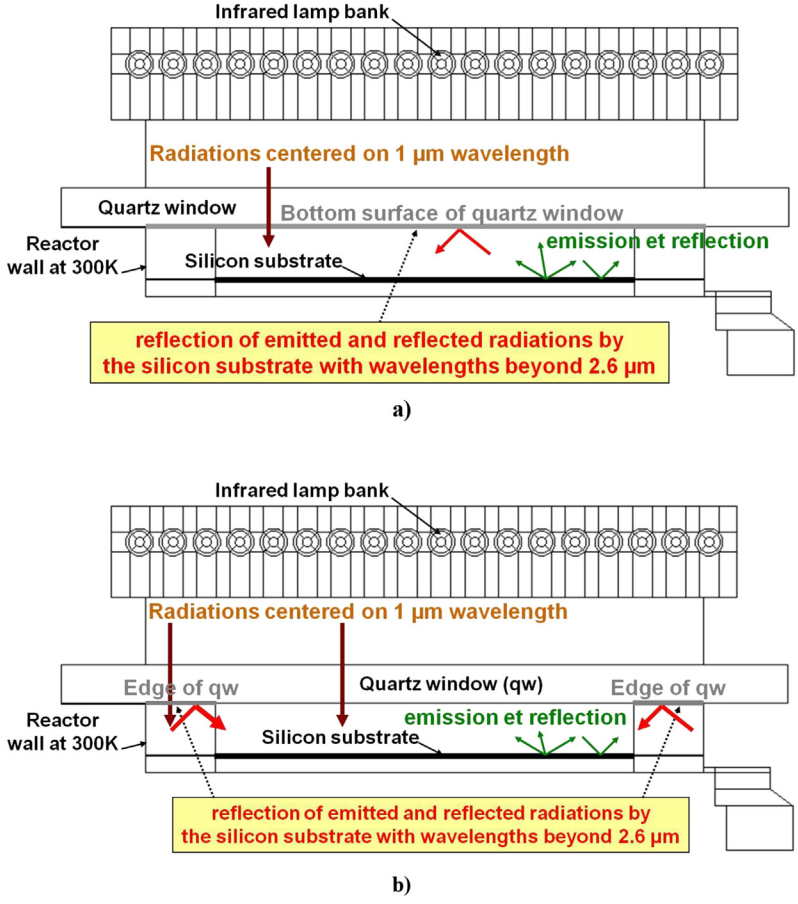

Fig. 6. First (a) and second (b) scheme to improve the temperature homogeneity of the wafer.

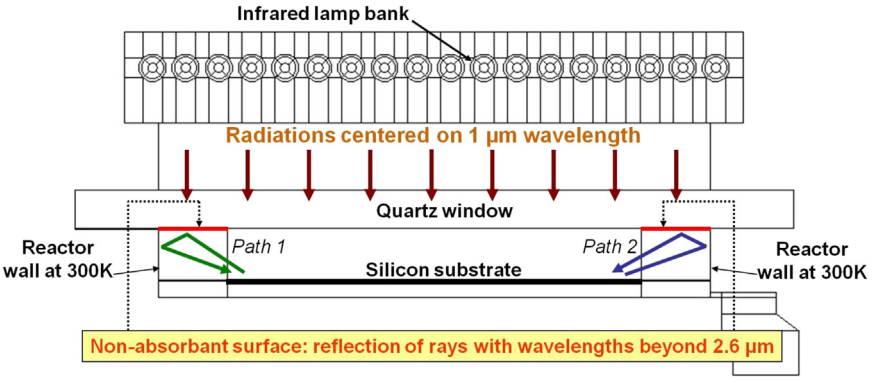

Fig. 7. Reflection of emitted rays by the edge of the wafer.

the central surface of the quartz window. Therefore, the radiative flux received by the wafer should be more homogeneous as the window temperature will be reduced namely in its centre.

For the second proposition (Fig. 8b), in the wavelength domain beyond 2.6 µm, the emitted and reflected radiations by the wafer at its centre are absorbed by the quartz window in its central area and one part is re-emitted towards the wafer. The flux emitted by the wafer at its edge is reflected by the surface of the window close to the reactor wall. The flux reflected by the window close to the reactor wall in direction of the edge of the wafer is expected to be in the same order of the one emitted by the quartz window in its central part, or even superior, to have a balance in the radiative fluxes for the wafer.

6. Implementation

The wanted radiative property for the lower surface of the quartz window is given in Fig. 9. The reflectivity and the transmissivity are provided according to wavelength. The emitted and reflected radiations having wavelengths beyond 2.6 µm by the wafer will be reflected and the ones emitted by the tungsten halogen lamps, centred at around 1 µm wavelength will be

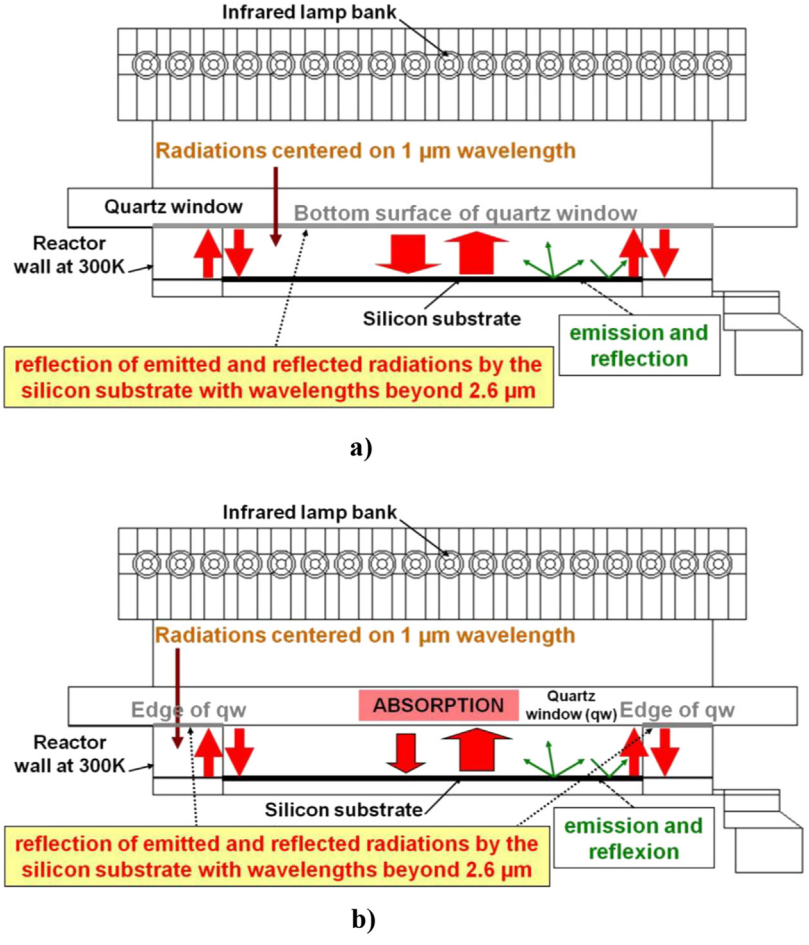

Fig. 8. Reasoning on radiative heat flux magnitudes.

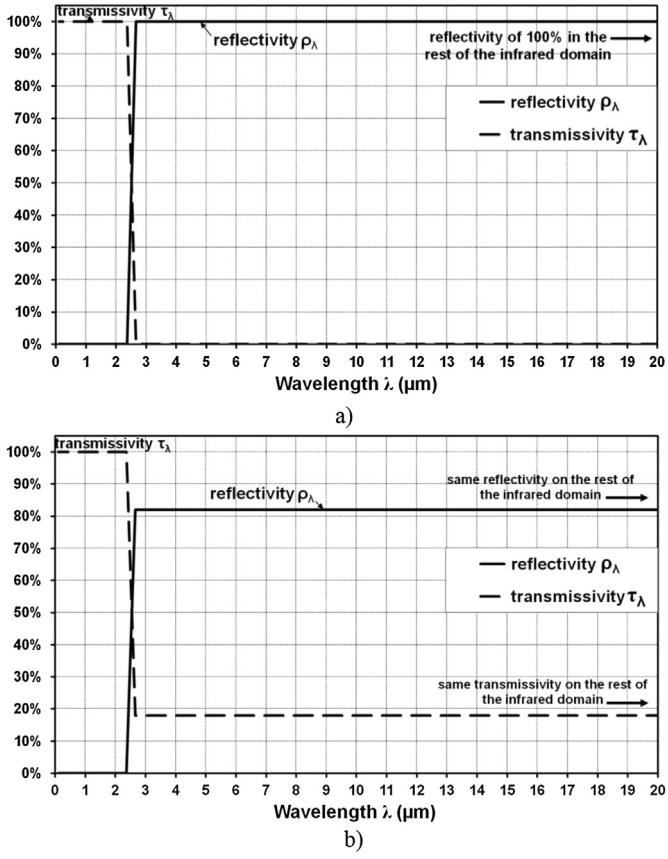

Fig. 9. Required radiative property on the underside surface of the window (a) with its eventual adjustment (b).

transmitted. The filter will be applied on the lower underside surface of the quartz window (Fig. 10a) and on the underside area of the quartz window close to the reactor wall which corresponds to a ring (Fig. 10b).

7. Simulation results

The wanted radiative property (filter) is entered for the lower surface property of the window in the two-dimensional model of the AS-One 150. Calculations are performed for the steady-state case for the same lamp wattages (10–30%).

7.1. Filter on the underside of the quartz window (solution 1)

The temperatures obtained at the centre of the window and at the centre of the wafer are compared with and without the filter on the underside surface of the quartz window (Fig. 11).

The temperature of the window is reduced by the presence of the filter. However, the difference is in the order of 10%. This small difference is due to the fact that the quartz window does not transmit all the incident radiations from the lamps (transmissivity of 95% for radiations centred at around 1 μm wavelength). As the calculations are realized for the steady-state case, for an infinite assumed time, the quartz window had had enough time to store heat, even though the window reflects radiations having wavelengths beyond 2.6 μm on its underside.

The filter enhances a decrease of the temperature of the window, but the temperature of the wafer becomes more elevated. The increase of the wafer temperature is very significant for powers above 15% because the radiations having wavelengths beyond 2.6 μm emitted and reflected by the wafer, which are reflected by the filter, are more important. The lamp power – wafer temperature correspondence is hence different from the one with a blank quartz window [38]. To appreciate the effect of the filter on the wafer temperature homogeneity, it is therefore more interesting to represent the temperature difference between its centre and its edge according to the temperature at its centre (Fig. 12). The temperature difference between the centre and the edge of the wafer is decreased by about 30 K for wafer temperatures below 1000 K and by 20 K for wafer temperatures above. The reduction of the wafer temperature differences with the filter is indeed verified.

7.2. Filter arranged in a ring on the underside of the quartz window (solution 2)

In the second configuration, the filter is applied as a ring close to the reactor wall on the underside of the window. The rest of the lower surface of the window, facing the wafer, has the radiative properties of quartz. The wafer temperature profiles are confronted in Fig. 13 for the window with and without the ring filter for three heating powers: a low one (10%), an average one (20%) and a high one (30%). The overall temperature of the wafer is also heightened with the ring filter which returns one part of the radiations emitted and reflected by the edge of the wafer towards the latter. The temperature difference between the centre and the edge of the wafer is reduced, namely for 20% lamp heating power, where the temperature dispersion is inferior to 1%. As expected, the temperature at the edge of the wafer is raised, so the reasoning is validated.

To appreciate better the effect of the ring filter, the temperature variations obtained according to the lamp heating powers are plotted in Fig. 14. The temperature difference between the centre and the edge of the wafer is reduced. The temperature distribution is the most homogeneous for medium powers (around 20%). For low heating powers (10% and 15%), the improvement is not as good because radiations emitted and reflected by the wafer with wavelengths beyond 2.6 μm are less important, which doesn't raise enough the temperature at the edge of the wafer after reflection on the ring filter. On the contrary, for high power (for example 30%), the temperature at the edge of the wafer is too high because the reflected radiations by the ring filter on the edge are too elevated. The compromise is found for medium powers.

8. Discussion

The temperature difference between the centre and the edge of the wafer according to the temperature at its centre is plotted in Fig. 15. The ring filter enables a more homogeneous temperature for the wafer with medium and high powers contrary to the filter on the entire underside surface of the window. For low powers, the temperature is more homogeneous with the filter on the entire underside surface because there is a better balance for the incident fluxes on the wafer. The application of a filter on the lower surface of the window would prevent the augmentation of the temperature of the quartz window which could limit the deposition on the lower surface of the window during rapid thermal chemical vapour deposition processes (RTCVD). Such depositions on the quartz window modify the signal received by the pyranometer which results in erroneous heating control.

For high lamp powers, a raised temperature at the edge of the wafer is observed because the reflectivity of the ring filter for wavelengths above 2.6 μm is too strong. This reflectivity has to be adjusted according to the used process to acquire uniform wafer temperature. Optimization with the lamp heating power has to be preliminary performed.

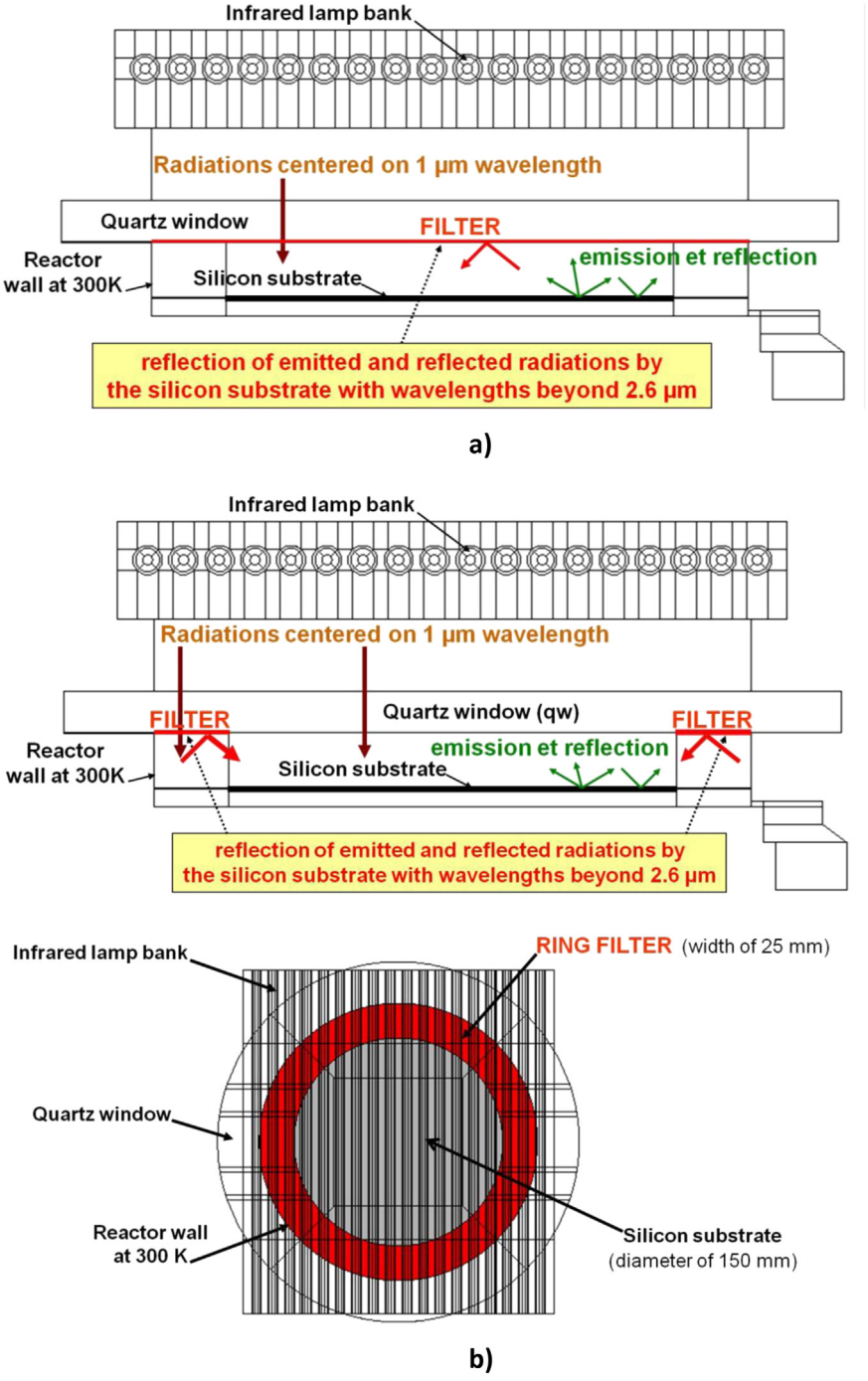

Fig. 10. The two configurations for the filter: entire surface (a) and ring configuration with view from below (b).

Compared to the solutions to improve the wafer temperature homogeneity quoted in the introductive part, the two proposed solutions are simple to implement. Besides, they do not involve a fluid flowing through a double window which absorbs one part of the infrared radiations emitted by the lamps to cool down the quartz window [13,50,51] or any arrangements in the chamber to select the radiations [52]. These solutions are only a simple modification of the surface property of the underside of the quartz window which can be realized by depositing thin-film layers on the underside surface of the quartz window with the help of a mask to adjust the shape of the layer. Thin-film layers deposited on glass or quartz substrates allow to perform specific functions according to the wavelength of the incident radiations [53]. The function that we wish to have on the lower surface of the window (Fig. 8) is the one of a low pass filter for transmissivity and a high pass one for the reflectivity with a cutoff at 2.6 µm wavelength. Transparent conductive oxides (TCO) deposited on glass or quartz would be suitable because they have properties similar to the ones of the wanted filter. They are thermally and chemically stable which would permit to avoid contamination in the reactor and they can be deposited on large areas [54,55]. For example, oxide films doped with fluorine or tin deposited on quartz substrates would have the required radiative properties [56,57].

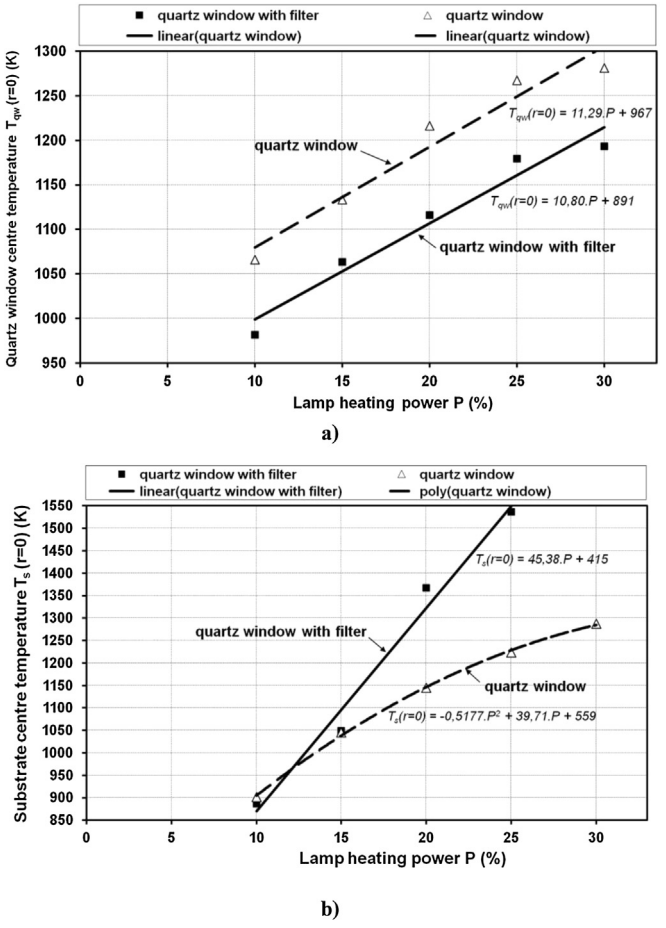

Fig. 11. Temperature at the centre of the quartz window (a) and at the centre of the substrate (b) according to the lamp heating power with and without the filter (solution 1) and at the centre of the substrate (b).

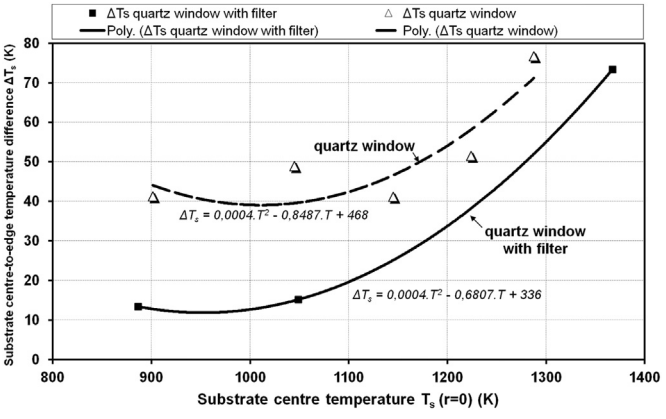

Fig. 12. Centre-to-edge temperature difference of the wafer according to its temperature at the centre with and without filter on the underside surface of the quartz window (solution 1).

9. Conclusion

The heating of a silicon wafer by tungsten filament halogen infrared lamps in a rapid thermal system is studied to explain the distribution of the wafer temperature. For this purpose, radiative transfers are simulated with the Monte Carlo method. The numerical simulations performed for the steady-state case without

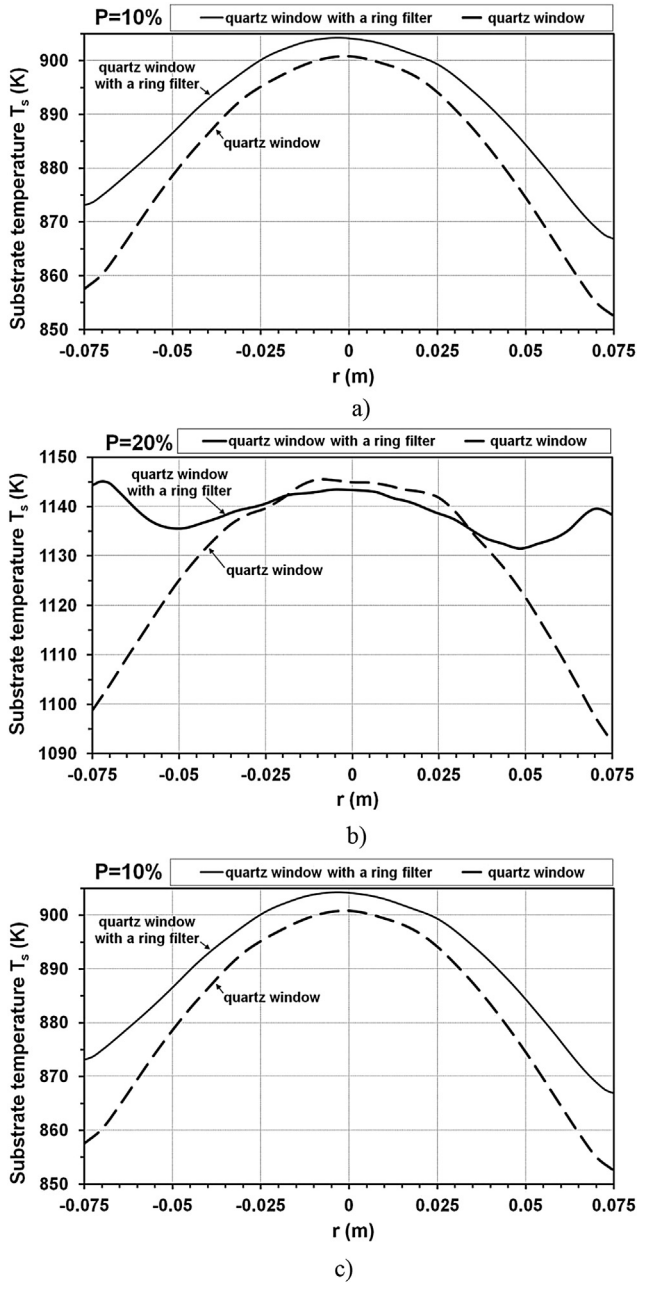

Fig. 13. Comparison of temperature profiles with and without the filter in a ring underside the quartz window (solution 2) for lamp heating power P of 10% (a), 20% (b) and 30% (c).

any optimization for different radiative properties of the substrate allowed to appreciate the close relationship between the temperature of the silicon wafer and the one of the quartz window. A radiative heat exchange by absorption-emission and reflection of radiations having wavelengths above 2.6 μm is highlighted and analyzed with the spectral properties of participating surfaces. The radiative fluxes conditioning the shape of the wafer temperature are identified and depicted in a four-phase scheme. From the latter, a modification of the surface property on the underside of the quartz window was recommended. The aim is to reflect the infrared radiations with wavelengths beyond 2.6 μm towards the wafer to cool down the quartz window or to confine in the area close to the reactor wall the radiations in order to raise the temperature at the edge of the wafer. Two configurations with the

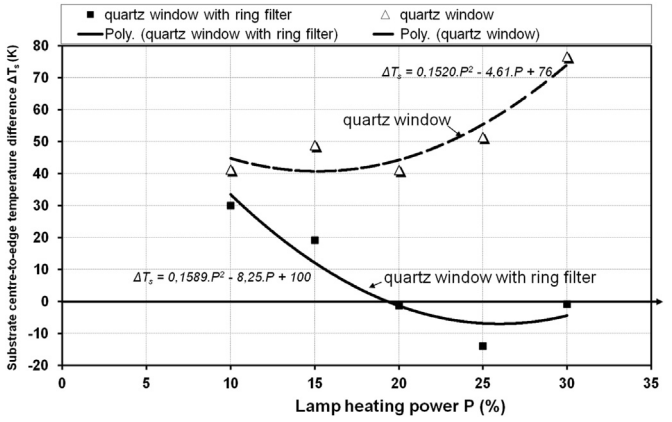

Fig. 14. Centre-to-edge temperature difference of the wafer the filter in a ring underside the quartz window (solution 2).

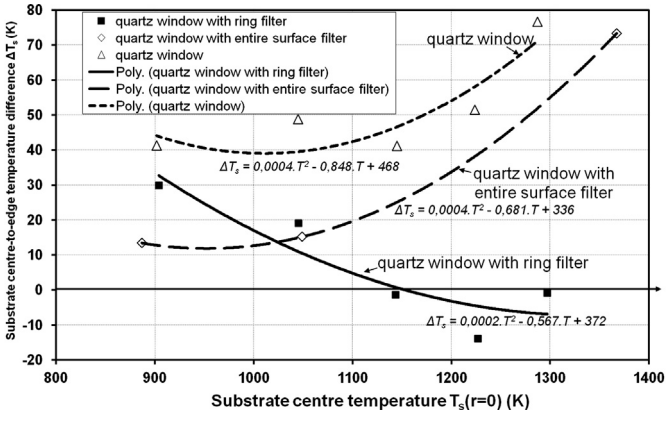

Fig. 15. Centre-to-edge temperature difference of the substrate according to its temperature at its centre for both the filter configurations and without filter.

property were then studied by numerical simulations: one where the filter is arranged over the entire underside surface of the window and the other where it is arranged in a ring close to the reactor wall. Calculation results show that both configurations allow a better homogeneity of the wafer temperature. The ring filter is optimal for medium and high lamp heating powers whereas the filter placed over the entire underside face is more suitable for low ones. The ring filter enables to uniform the temperature of the silicon wafer with less than 1% dispersion. The use of a filter applied on the entire lower surface also permits to limit the overheating of the quartz window. For an experimental implementation, the filter could be realized by depositing a transparent conductive oxide coating (TCO: Transparent Conducting Oxide) on the underside of the quartz window. The next step is to carry out simulations for transient evolutions to adjust the reflectivity of the filter according to various rapid thermal processes. Further, the manufacturing of coated quartz windows and wafer temperature measurements will have to be realized to confirm the promising simulation results.

Acknowledgements

The authors thank the Centre des Resources Technologiques de Sénart (CRTS) for the support and the company AnnealSys and particularly the director, Mr. Frank Laporte for his aid and for providing an AS-One 150 equipment for the present study. They also wish to thank Mrs. Wilhelmina Logerais, a native speaker, for her help with English.

References

[1] V.E. Borisenko, P.J. Hesketh, Rapid Thermal Processing of Semiconductors, Plenum Press, New York, 1997.
[2] B. Mattson, P.J. Timans, S.P. Tay, D.J. Devine, J. Kim, in: D.P. DeWitt, J. Gelpey, B. Lojek, Z. Nenyei (Eds.), Proceedings on 9th International Conference on Advanced Thermal Processing of Semiconductors-RTP 2001, 2001, p. 13.
[3] S.C. Karle, A.D. Shaligram, Feasibility study on rapid thermal processing, Solid-State Electron. 53 (2009) 1046–1049.
[4] B. Lojek, Early history of rapid thermal processing, in: Proc. of 1999 IEEE Int. Conf. on Adv. Thermal Proc. of Semicon, RTP'99, 1999, pp. 292–317.
[5] J. Niess, S. Paul, S. Buschbaum, P. Schmid, W. Lerch, Mainstream rapid thermal processing for source-drain engineering from first applications to latest results, Mater. Sci. Eng. B Solid-State Mater. Adv. Technol. 114–115 (2004) 141–150.
[6] C.P. Malhotra, R.L. Mahajan, W.S. Sampath, K.L. Barth, R.A. Enzenroth, Control of temperature uniformity during the manufacture of stable thin-film photovoltaic devices, Int. J. Heat Mass Transf. 49 (2006) 2840–2850.
[7] W.A. Keenan, W.H. Johnson, D. Hodul, D. Mordo, RTP temperature uniformity mapping, Nucl. Instrum. Methods Phys. Res. B 55 (1991) 269–274.
[8] C. Schaper, Y. Cho, P. Park, S. Norman, P. Gyugyi, G. Hoffmann, S. Balemi, S. Boyd, G. Franklin, T. Kailath, K. Saraswat, Modeling and control of rapid thermal processing, in: SPIE Proceedings of the Rapid Thermal and Integrated Processing, 1991.
[9] M. Glück, W. Lerch, D. Löffelmacher, M. Hauf, U. Kreiser, Challenges and current status in 300 mm rapid thermal processing, Microelectron. Eng. 45 (1999) 237–246.
[10] C.J. Huang, C.C. Yu, S.H. Shen, Selection of measurement locations for the control of rapid thermal processor, Automatica 36 (2000) 705–715.
[11] D. Biro, R. Preu, O. Schultz, S. Peters, D.M. Huljic, D. Zickermann, R. Schindler, R. Ludemann, G. Willeke, Advanced diffusion system for low contamination in-line rapid thermal processing of silicon solar cells, Sol. Energy Mater. Sol. Cells 74 (2002) 35–41.
[12] S.J. Kim, Y.M. Cho, Optimal design of a rapid thermal processor via physics-based modeling and convex optimization, Control Eng. Pract. 10 (2002) 1199–1210.
[13] E. Dassau, B. Grosman, D.R. Lewin, Modelling and temperature control of rapid thermal processing, Comput. Chem. Eng. 30 (2006) 686–697.
[14] J.C. Jeng, W.C. Chen, Control strategies for thermal budget and temperature uniformity in spike rapid thermal processing systems, Comput. Chem. Eng. 57 (2013) 141–150.
[15] H. Hovel, M. Almonte, P. Tsai, J.D. Lee, S. Maurer, R. Kleinhenz, D. Schepis, R. Murphy, P. Ronsheim, A. Domenicucci, J. Bettinger, D. Sadana, Qualification of 300 mm SOI CMOS substrate material: readiness for development and manufacturing, Solid-State Electron. 48 (2004) 1065–1072.
[16] P. Vandenabeele, K. Maex, Modelling of rapid thermal processing, Microelectron. Eng. 10 (1991) 207–216.
[17] A.H. Wang, Y.H. Niu, T.J. Chen, P.F. Hsu, Effects of thermal transport properties on temperature distribution within silicon wafer, J. Central South Univ. 21 (4) (2014) 1402–1410.
[18] D.S. Ballance, B. Bierman, J.V. Tietz, Gas introduction showerhead for an RTP chamber with upper and lower transparent plates and gas flow there between, U. S. Pat. 5781693 A, 1998.
[19] P.O. Logerais, M. Girtan, A. Bouteville, Influence of the quartz window in a rapid thermal processing apparatus, J. Optoelectron. Adv. Mater. 8 (1) (2006) 139–143.
[20] N. Yoshio, R. Doering, Handbook of Semiconductor Manufacturing Technology, Marcel Dekker, New York, 2000.
[21] A.J. Silva Neto, M.J. Fordham, W.J. Kiether, F.Y. Sorrell, Rapid thermal processing furnace with three heating zones, Revista Brasileira De Ciencias Mecanicas/Journal Braz. Soc. Mech. Sci. 20 (1998) 532–541.
[22] N. Acharya, V. Kirtikar, S. Shooshtarian, H. Doan, P.J. Timans, K.S. Balakrishnan, K.L. Knutson, Uniformity optimization techniques for rapid thermal processing systems, IEEE Trans. Semicond. Manuf. 14 (3) (2001) 218–226.
[23] W.R. Aderhold, A. Hunter, J.M. Ranish, System for non radial temperature control for rotating substrates, US Patent 20140220710 A1, 2014.
[24] A. Tillmann, S. Buschbaum, S. Frigge, U. Kreiser, D. Löffelmacher, T. Theilig, Modelling and off-line optimization of a 300 mm rapid thermal processing system, Mater. Sci. Semicond. Process. 1 (1998) 181–186.
[25] W.S. Yoo, A.J. Atanos, J.F. Daviet, Susceptor-based rapid thermal processing system and its suicide application, Jpn. J. Appl. Phys. Part 2: Lett. 37 (10 part A) (1998) L1135–L1137.
[26] R. Kakoschke, E. Bussmann, H. Foell, Modelling of wafer heating during rapid thermal processing, Appl. Phys. A: Solids Surfaces 50 (1990) 141–150.
[27] K. Knutson, S.A. Campbell, F. Dunn, Three dimensional temperature uniformity modelling of a rapid thermal processing chamber, in: Materials Research Society Symposium Proceedings, vol. 303, 1993, pp. 211–215.
[28] L. Plévert, Cristallisation par recuit rapide du silicium amorphe sur verre, thèse de doctorat, Université de Rennes I, 1995.

[29] C.K. Chao, S.Y. Hung, C.C. Yu, The effect of lamps radius on thermal stresses for rapid thermal processing system, J. Manuf. Sci. Eng. 125 (2003) 504–511.
[30] A. Wacher, B.R. Seymour, A radiation model of a rapid thermal processing system, Mathematics-in-Industry Case Stud. J. 3 (2011) 1–18.
[31] K.S. Balakrishnan, T.F. Edgar, Model-based control in rapid thermal processing, Thin Solid Films 365 (2000) 322–333.
[32] H. Habuka, T. Otsuka, M. Mayusumi, M. Shimada, K. Okuyama, A direct approach for evaluating the thermal condition of a silicon substrate under infrared rays and specular reflectors, J. Electrochem. Soc. 146 (2) (1999) 713–718.
[33] J. Liu, Y.S. Chen, Prediction of surface radiative heat transfer using the modified discrete transfer method, Numer. Heat Transf. Part B Fundam. 38 (4) (2000) 353–367.
[34] Y. Yu, P. Ming, S. Zhou, Numerical study on transient heat transfer of a quartz lamp heating system, Math. Problems Eng. 2014 (2014), http://dx.doi.org/10.1155/2014/530476. Article ID 530476.
[35] A. Kersch, W.J. Morokoff, Transport Simulation in Microelectronics, Birkhauser, Bâle, 1995.
[36] A. Kersch, T. Schafbauer, Thermal modelling of RTP and RTCVD processes, Thin Solid Films 365 (2) (2000) 307–321.
[37] Y.H. Zhou, Y.J. Shen, Z.M. Zhang, B.K. Tsai, D.P. DeWitt, A Monte Carlo model for predicting the effective emissivity of the silicon wafer in rapid thermal processing furnaces, Int. J. Heat Mass Transf. 45 (2002) 1945–1949.
[38] P.O. Logerais, D. Chapron, J. Garnier, A. Bouteville, Validation of a Rapid Thermal Processing model in steady-state, Microelectron. Eng. 85 (2008) 2282–2289.
[39] P.O. Logerais, R. Khelalfa, O. Riou, J.F. Durastanti, A. Bouteville, Influence of the window thermal diffusivity on the silicon wafer temperature in a rapid thermal system, Heat. Transf. Eng. 36 (13) (2015).
[40] P.O. Logerais, D. Chapron, A. Bouteville, Transient simulations of a rapid thermal processing apparatus, J. Optoelectron. Adv. Mater. 9 (4) (2007) 1082–1086.
[41] AnnealSys : www.annealsys.com.
[42] H.V. Versteeg, W. Malalasekera, An Introduction to Computational Fluid Dynamics, the Finite Volume Method, Longman, Londres, 1995.
[43] M.F. Modest, Radiative Heat Transfer, McGraw-Hill, New York, 1993.
[44] S. Mazumder, A. Kersch, A fast Monte Carlo scheme for thermal radiation in semiconductor processing applications, Numer. Heat Transf. Part B: Fundam. 37 (2000) 185–199.
[45] C.J. Glassbrenner, G.A. Slack, Thermal conductivity of silicon and Germanium from 3°K to the melting point, Phys. Rev. 134 (4A) (1964) 1058–1069.
[46] A.S. Okhotin, A.S. Pushkarskii, V.V. Gorbachev, Thermophysical Properties of Semiconductors (In Russian), Atom, Russia, 1972. Moscow.
[47] ESI group : www.esi-group.com .
[48] CFD Research Corporation, CFD'ACE (U) Module Manual, Version 2013, 2013. Huntsville.
[49] E.D. Palik, Handbook of Optical Constants of Solids, Academic Press, New York, 1998.
[50] A. Slaoui, S. Bourdais, G. Beaucarne, J. Poortmans, S. Reber, Polycrystalline silicon solar cells on multiple substrates, Sol. Energy Mater. Sol. Cells 71 (2) (2002) 245–252.
[51] C.P. Yin, C.C. Hsiao, T.F. Lin, Improvement in substrate temperature uniformity and flow pattern in a lamp heated rapid thermal processor, J. Cryst. Growth 217 (2000) 201–210.
[52] Timans, J.P., Devine, D.J., Lee, Y.J., Hu, Y.Z., Bordiga, P.C., Selective reflectivity process chamber with customized wavelength response and method, United States Patent 07115837, october 3rd 2006.
[53] H.A. Macleod, Thin-films Optical Filters, Institute of Physics Publishing, Bristol and Philadelphia, 2001.
[54] J.G. Lu, T. Kawaharamura, H. Nishinaka, Y. Kamada, T. Ohshima, S. Fujita, ZnO-based thin films synthesized by atmospheric pressure mist chemical vapor deposition, J. Cryst. Growth 299 (1) (2007) 1–10.
[55] H. Lin, T. Jin, A. Dmytruk, M. Saito, T. Yazawa, Preparation of a porous ITO electrode, J. Photochem. Photobiol. A: Chem. 164 (1–3) (2004) 173–177.
[56] S. Shanthi, C. Subramanian, P. Ramasamy, Investigations on the optical properties of undoped, fluorine doped and antimony doped tin oxide films, Cryst. Res. Technol. 34 (8) (1999) 1037–1046.
[57] F.F. Ngaffo, A.P. Caricato, A. Fazzi, M. Fernandez, S. Lattante, M. Martino, F. Romano, Deposition of ITO films on SiO_2 substrates, Appl. Surf. Sci. 248 (1–4) (2005) 428–432.

Nomenclature

A: patch area *i*, m^2
e: specific internal energy, J
E: emissive power, W m^{-2}
E: total specific energy, J
f: external force vector per unit volume, N m^{-3}
k: absorption index
k: thermal conductivity, W m^{-1} K^{-1}
M: exchange matrix
n: refractive index
$\ddot{n}$: complex refractive index
N_s: total number of patches
p: static pressure, *Pa*
P: probability density function
q: radiative heat flux density, W m^{-2}
Q: radiative heat flux, *W*
r: radial coordinate, m
R: cumulated distribution function
S: source term
T: temperature, *K*
T_j: mean temperature of patch *j*, *K*
v: velocity, m s^{-1}
z: longitudinal coordinate

Greek symbols

α: absorptivity
δ: Kronecker symbol
ε: emissivity
θ: angle,°
θ: angular coordinate,°
$\boldsymbol{\theta}$: reduced temperature
λ: wavelength, m
$\boldsymbol{\rho}$: density, kg m^{-3}
ρ: reflectivity
τ: transmissivity
$\boldsymbol{\tau}$: viscous stress tensor, *Pa*

Indices

e: energy
i,j: patch
qw: quartz window
r,θ,z: cylindrical coordinates
s: substrate (wafer)
λ: wavelength

Constant

σ: Stephan–Boltzmann constant, $5.669 \cdot 10^{-8}$ W m^{-2} K^{-4}